Nd^{3+}-doped $Ca_3Ga_2Ge_3O_{12}$ garnet: A new optical pressure sensor

U. R. Rodríguez-Mendoza,[1,a)] S. F. León-Luis,[1] J. E. Muñoz-Santiuste,[2] D. Jaque,[3] and V. Lavín[1]

[1]*Dpto. de Física Fundamental y Experimental, Electrónica y Sistemas, and MALTA Consolider Team, Universidad de La Laguna, 38200 San Cristóbal de La Laguna, Santa Cruz de Tenerife, Spain*
[2]*Dpto. de Física Aplicada, and MALTA Consolider Team, Escuela Politécnica Superior, Universidad Carlos III de Madrid, Avda. del Mediterráneo, 20913 Leganés, Madrid, Spain*
[3]*CGIEL, and Departamento de Física de Materiales, Facultad de Ciencias, Universidad Autónoma de Madrid, 28049 Cantoblanco, Madrid, Spain*

(Received 23 January 2013; accepted 20 May 2013; published online 7 June 2013)

A pressure-induced shift of the emission spectrum corresponding to the near infrared $^4F_{3/2} \rightarrow {}^4I_{9/2}$ transition of Nd^{3+} ions in a calcium gadolinium germanium garnet was obtained in the interval from ambient conditions up to 23 GPa in order to test its suitability as an optical pressure sensor. Although several Nd^{3+} non-equivalent centers are present in this garnet, which complicates the assignation of the optical transitions, the R_1,$R_2 \rightarrow Z_5$ transitions are unequivocally characterised and fit the requirements of an ideal optical pressure sensor. Results obtained for these emission peaks indicate large pressure coefficients of -8.8 and $-10.8\,cm^{-1}\,GPa^{-1}$; meanwhile, the rest of the R_1,$R_2 \rightarrow Z_{1-4}$ emissions remain almost unchanged under pressure. This behaviour is ascribed to the influence of the crystal-field at high pressure on the Z_5 Stark level of the ground state and can be easily reproduced exclusively by varying the cubic term of fourth rank of the crystal-field Hamiltonian, which accounts for the Nd^{3+} ions and is related to medium Nd^{3+}-oxygen distances. These coefficients are larger than those found for the R-lines of Cr^{3+} in ruby, $-7.56\,cm^{-1}\,GPa^{-1}$, suggesting that this system may be a good candidate for a luminescence pressure sensor. [http://dx.doi.org/10.1063/1.4809217]

I. INTRODUCTION

Matter under extreme pressure and/or temperature conditions is the subject of multidisciplinary studies that join diverse fields as physics, chemistry, geology, material science, microbiology, or food technology.[1–4] One of the fundamental goals of the high pressure technique is to mimic processes and phenomena that occur in the interior of the Earth and other planetary objects, such as phase transitions, chemical reactions, or microbiological activity, and to understand their physical, chemical, geological, and biological foundations and implications. In particular, the high pressure technique applied to optical spectroscopy provides a number of advantages over other techniques at ambient pressure conditions.[3,4] On one hand, it provides a unique insight into the electronic structure and optical properties of materials doped with transition metals or rare earth ions, since it can vary the structure, the coordination environment and, consequently, the electric, magnetic, vibrational, and optical properties. On the other hand, by reducing the volume of the sample, it allows a wide range of structures and bindings of a particular chemical composition to be studied.[3,4]

Solid material can be compressed at high pressure with the help of an anvil cell.[1,2] Choosing the type of anvil cell depends on the pressure range required. The most commonly used are sapphire, moissanite, and, especially, diamond. These devices allow a variety of optical, electrical, X-ray, and other studies over a wide range of the electromagnetic spectrum to be carried out at low and high temperature and high magnetic fields. A pre-indented metal gasket with a centred hole, together with both anvils, constitutes the hydrostatic chamber in which the sample, the hydrostatic medium, and the pressure sensor should be inserted. In order to achieve very high pressures, this chamber should be very small, typically 100 μm in diameter and 50 μm in height. The choice of the hydrostatic medium depends both on its chemical reactivity with the sample and on its hydrostaticity range. The determination of the pressure inside the hydrostatic sample chamber of the cell requires a calibrated standard. It is quite common to determine the working pressure through an *in situ*, indirect measurement of the calibrated pressure-sensitive luminescence of an optically active ion, i.e., transition metal or rare earth, in a micro-sized crystalline host located in the sample chamber.

The ideal optical pressure sensor for high pressure techniques needs to meet some general requirements, described by Barnett *et al.*[5] as: (i) a single emitting line; (ii) with no significant broadening or weakening and little or no surrounding background; (iii) with a large shift with pressure $d\lambda/dP$; (iv) a small temperature dependent line shift $d\lambda/dT$; (v) for high sensitivity and precision, its linewidth Γ should be small compared to the line shift, i.e., low $\Gamma^{-1}d\lambda/dP$ factor; and, finally, (vi) the host lattice should be highly stable at high pressures and temperatures.

The most commonly used luminescence pressure sensor is the Cr^{3+}:Al_2O_3 crystal (ruby),[3,4,6] monitoring the wavelength red-shift of the lower energy R_1 emitting line ($^2E \rightarrow {}^4A_2$) with pressure. Its strong luminescence efficiency at around 700 nm

[a)]Author to whom correspondence should be addressed. Electronic mail: urguez@ull.edu.es

and the strong line shift relative to its linewidth that occurs when pressure is increased are its most important features. Moreover, it can be easily measured by exciting with commercial lasers (Ar^+, violet and blue laser diode, or green diode-pumped solid state laser) and recorded with a conventional highly efficient photomultiplier tube. However, it has several drawbacks: temperature-induced broadening, which produces a strong overlap with the emission from the R_2 line; luminescence quenching, which limits its application to below 500 °C; low pressure sensitivity below 1 GPa, a range especially important for life-related high pressure research; the signal overlap of the sample's luminescence with the strong luminescence of ruby; and finally, the need to change the detector if the emission of the sample lies in other spectral range than the sensor. Thus, new sensors should resolve these problems, while preserving the advantages of ruby.

Due to all these requirements, special attention has been paid to rare-earth based sensors because the shielding of the 4f-electrons produces very sharp absorption and emission lines in the UV-VIS-near-infrared (NIR) optical range that are less sensitive to the environment compared to those of the 3d electrons of Cr^{3+}. In this sense, the luminescence in systems such as Nd^{3+}-doped $YAlO_3$ have been tested in the NIR range, studying the pressure shifts of the $R_2 \rightarrow Z_2$ line of the $^4F_{3/2} \rightarrow {}^4I_{9/2}$ transition.[5] Particularly interesting are the high pressure studies carried out in 1990s by Hua *et al.*[7] in Nd^{3+}-doped yttrium gadolinium (YAG), gadolinium gallium (GGG), and gadolinium scandium gallium (GSGG) garnets, the latter co-doped with Cr^{3+}, in which special attention was paid to the R_1,$R_2 \rightarrow Z_1$ lines of the $^4F_{3/2} \rightarrow {}^4I_{9/2}$ transition. More complete high pressure studies were later carried out on similar garnets doped with Nd^{3+}, in particular lanthanum lutetium gallium garnets (LLGG),[8] gadolinium GSGG co-doped with Cr^{3+},[9] yttrium aluminium garnets (YAG),[10] and gadolinium gallium garnets (GGG),[11] focusing on the R_1,$R_2 \rightarrow Z_5$ lines of the $^4F_{3/2} \rightarrow {}^4I_{9/2}$ transition, in which sensor applications have been found. Moreover, in the latter study, an extensive analysis of the crystal-field interaction in the environment of the rare earth ion was carried out.

In this paper, we study the high pressure luminescence properties of Nd^{3+} in a calcium gallium germanium garnet crystal (Nd^{3+}:CGGG), analysing in detail the $^4F_{3/2} \rightarrow {}^4I_{9/2}$ emission. The advantage of this crystal over other garnets is that it possesses a lower melting point and is therefore less expensive to manufacture.[12] The study of the evolution of its NIR emission spectrum when pressure increases, particularly the R_1,$R_2 \rightarrow Z_5$ lines of the $^4F_{3/2} \rightarrow {}^4I_{9/2}$ transition, indicates that this crystal can be used as a pressure sensor in the NIR.

II. EXPERIMENTAL

The Nd^{3+}-doped $Ca_3Ga_2Ge_3O_{12}$ (Nd^{3+}:CGGG) crystal was grown by the Czochralski technique. The luminescence of the Nd^{3+} ions was excited either by the 488 nm line of an Ar^+ laser (Spectra Physics 2065A-66 Beamlok) or the radiation of a 532 nm diode-pumped solid state laser and recorded using a 0.75 m single grating monochromator (Spex 750M) equipped with a cooled NIR extended photomultiplier (Hamamatsu R-5102), and using the lock-in technique (EG&G Princeton Applied Research model 5210). High pressure was generated with a miniature diamond anvil cell (mini-DAC) designed at The University of Paderborn (Germany). Four different high pressure experiments were performed in sample chambers of typical dimensions of $Ø = 150\,\mu m$ and $h = 70\mu m$ using $\sim 10\,\mu m$ ruby chips as pressure calibrant. A 16:4:1 methanol-ethanol-water mixture served as pressure medium, providing hydrostatic pressures of up to ~15 GPa. Low temperature experiments between 77 K and room temperature were achieved by mounting the mini-DAC in a continuous closed He cycle cryostat (PC202 AF Advanced Research System ARS).

III. RESULTS AND DISCUSSIONS

A. Ambient- and high-pressure luminescence

For optical applications, it is of particular interest to analyse the local structure around the rare earth ions in the matrix, since it rules the fine structure splitting of the free-ion multiplets and the forced intra-configurational 4f-4f electric-dipole transition probabilities. Garnet crystals belong to the Ia-3d cubic space group and have the general chemical formula $A_3B_2C_3O_{12}$, where A denotes the dodecahedral, B the octahedral, and C the tetrahedral sites in the lattice.[13] For the Nd^{3+}:$Ca_3Ga_2Ge_3O_{12}$ (CGGG) crystal, the Ca^{2+} ions are located in dodecahedral sites, and the Ga^{3+} and Ge^{4+} ions occupy octahedral and tetrahedral sites, respectively. The Nd^{3+} ion substitutes the Ca^{2+} ion in the dodecahedral site, and is surrounded by 8 oxygen ligands with a distorted cubic symmetry that will rise to a real D_2 orthorhombic local site symmetry.[13,14] Moreover, the excess charge of the Nd^{3+} ions can be compensated by substituting Ge^{4+} ions with Ga^{3+} ions, as suggested by Eskov *et al.*[15] Up to six different non-equivalent sites for the Nd^{3+} ions will be generated.[16,17] Therefore, the crystal-field interaction acting on the Nd^{3+} ions has such a low symmetry that it will completely lift the degeneracy of the $^{2S+1}L_J$ multiplets of the free-Nd^{3+} ion energy level diagram and split them into J+1/2 crystal-field, or Stark, levels according to the double Kramer degeneracy. The energy level scheme of the Nd^{3+} ion is very similar for the family of garnet crystals (see Fig. 1), and no large changes in energy are expected for the Stark levels involving the $^4F_{3/2} \rightarrow {}^4I_{9/2}$ transition of interest for a pressure sensor.

The starting point is the double cubic group, which splits the ground $^4I_{9/2}$ term in three levels, whose irreducible representations are denoted by $\Gamma_6 + 2\Gamma_8$, while keeping the lowest emitting $^4F_{3/2}$ level as a singlet, denoted by Γ_8 (see Fig. 1).[18] The orthorhombic distortion, superimposed on the main cubic field, lifts the remaining degeneracy and each Γ_8 level splits into two Stark doublets. As a result, the $\Gamma_8(^4F_{3/2})$ singlet splits into the R_1 and R_2 Stark levels, and the $^4I_{9/2}$ state appears structured as four levels (Z_1 to Z_4), paired two on two (coming from $2\Gamma_8$), with the last Z_5 Stark level (coming from Γ_6) slightly further away. The energy level scheme is depicted in Fig. 1, taking the Z_1 as the zero energy reference Stark level.

In this context, up to ten peaks may appear for each non-equivalent site, corresponding to transitions from the two R_i Starks of the $^4F_{3/2}$ state to the five Z_j Stark levels of

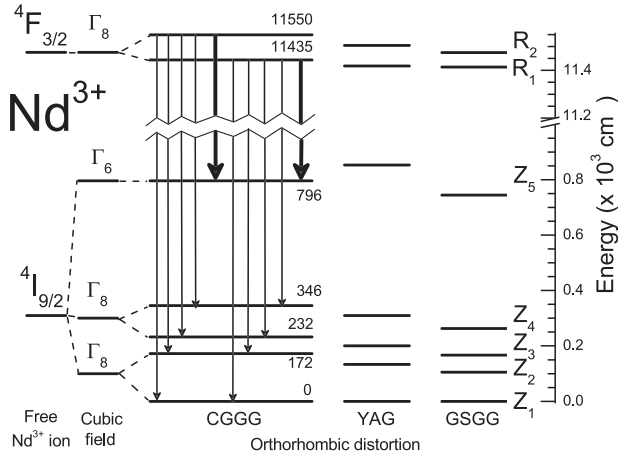

FIG. 1. Partial energy level diagram of the Nd^{3+} ion in CGGG, GSGG,[9] and YAG[10] garnets at ambient pressure corresponding to the $^4F_{3/2}$ and $^4I_{9/2}$ free-Nd^{3+} multiplets and the breakdown of their degeneracy into three and five Stark levels in cubic and orthorhombic-distorted environments, respectively. Due to the multi-site nature of the CGGG garnet, the energy of each Nd^{3+} Stark level indicated in the figure is averaged. The transitions between the $^4F_{3/2}$ and $^4I_{9/2}$ Stark levels are also given.

the $^4I_{9/2}$ ground state, which may complicate the resolution of the peaks and the identification of the transitions. At ambient conditions, two main parts of the luminescence spectrum can be distinguished (see Fig. 2): the first, ranging from 11 000 cm^{-1} to 11 600 cm^{-1} has a complex structure of peaks; and the second, composed of two high intensity peaks red-shifted from the rest around 300 cm^{-1} and easily identified as the R_1,$R_2 \rightarrow Z_5$ transitions.

Due to the fact that the R_1 and R_2 Stark levels are as close in energy as 100 cm^{-1} at ambient pressure, they can be treated as thermalized levels. Thus their relative populations follow a Maxwell-Boltzmann distribution, which predicts that the population of the R_2 upper level will decrease when the temperature decreases,[10] and consequently a quenching of the intensity of the R_2 emissions is expected respect to that of the R_1 emissions. Taking advantage of this feature, low temperature spectra were measured in order to identify those transitions associated to the R_1 and R_2 emissions by simply comparing the emission spectra of the $^4F_{3/2} \rightarrow {}^4I_{9/2}$ band at RT and at 77 K, both at ambient pressure (see Fig. 2). The quenching of the intensity of the bands corresponding to the $R_2 \rightarrow Z_j$ emissions is clearly observed for the low temperature spectrum, which allows us to identify all the $R_i \rightarrow Z_j$ transitions.

Moreover, slight differences can also be observed in the position and linewidths of these bands as a function of temperature. It is worth noting that despite the six non-equivalent sites found for the Nd^{3+} ions in the CGGG garnet structure,[16,17] the emission spectra of these transitions do not change significantly with the excitation pumping wavelength, after testing with four different lines of the Ar^+ laser and a 532 nm laser diode radiation. Thus the average positions at ambient conditions have been selected in order to elaborate a partial energy diagram (see Fig. 1).

The room temperature emission spectra of the Nd^{3+} ions in the CGGG garnet crystal associated with the $^4F_{3/2} \rightarrow {}^4I_{9/2}$ transition are presented in Fig. 3 as a function of pressure from ambient conditions up to 23 GPa. It is worth noting that inhomogeneous broadening increases for all the emission peaks above 15 GPa, which can be associated with the initial stages of loss of the hydrostatic condition of the transmitting medium in the pressure chamber, checked by analysing the broadening of the ruby lines. This fact, along with the overlapping of the $R_{1,2} \rightarrow Z_j$ (j = 1-4) transitions, makes the identification of the emission peaks at high pressure a difficult task. However, the main feature is that the most sensitive transitions to pressure are those between the R_1, R_2, and the

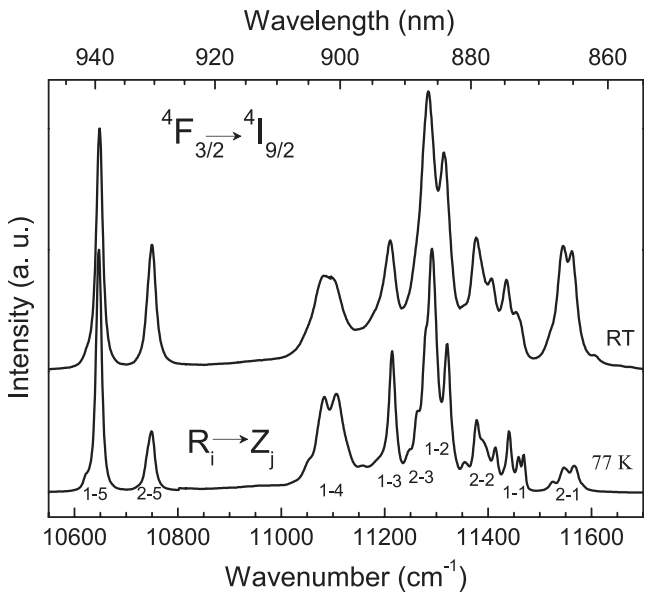

FIG. 2. Ambient pressure emission spectra of the $^4F_{3/2} \rightarrow {}^4I_{9/2}$ transition at RT and 77 K. The identification of the $R_{1,2} \rightarrow Z_{1\text{-}5}$ transitions is also given.

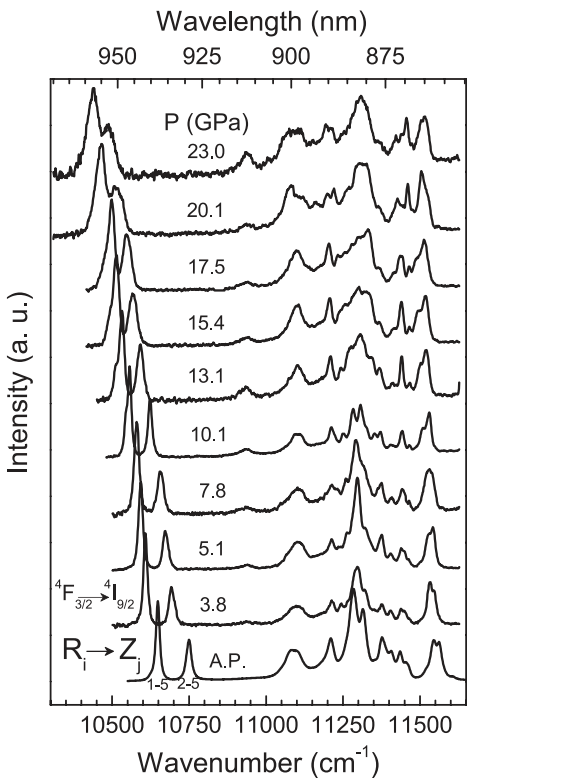

FIG. 3. Room temperature emission spectra of the $^4F_{3/2} \rightarrow {}^4I_{9/2}$ transition as a function of pressure.

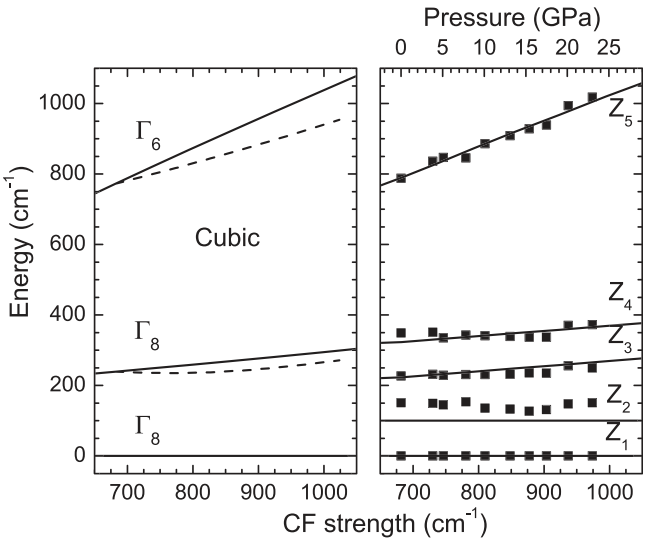

FIG. 4. (Left) The dependence of the $^4I_{9/2}$ cubic splitting on the cubic B_0^{4c} and B_0^{6c} CF parameters (solid lines) in the range of values of the overall CF strength for the CGGG garnet under study from ambient pressure up to 23 GPa. The dependence only on the B_0^{4c} CF parameter (dotted lines) is also given. (Right) Stark energy levels (■) of the $^4I_{9/2}$ ground state obtained from the emission spectra under pressure. Solid lines are obtained by superimposing a constant orthorhombic splitting ($\sim$100 cm^{-1}) to the Γ_8 cubic energy levels (see text for details).

Z_5 Stark levels, which show significant red-shifts, meanwhile the rest of the transitions do not change significantly, except the $R_2 \rightarrow Z_1$ which has a slight red-shift. The Stark energy levels of the $^4I_{9/2}$ ground state obtained from the emission spectra as a function of pressure are given in Fig. 4(right). From the perspective of potential sensor applications, Fig. 3 shows that the emissions associated with the R_1,$R_2 \rightarrow Z_5$ transitions seem to meet the requirements of the ideal optical pressure sensor described previously,[5] i.e., they are single and intense peaks, with small linewidths, large pressure coefficients ($d\lambda/dP$), there is no appreciable surrounding background and no phase transition takes place in the pressure range studied.

B. Crystal-field analysis

The shifts of the emission peaks of the Nd^{3+} ion can be correlated to variations in the energies of the $^{2S+1}L_J$ states and their hyperfine structure with pressure. Microscopically, these pressure-induced changes are related to variations of three major interactions, i.e., the Coulomb repulsion and the spin-orbit coupling, mainly responsible for the shift of the barycenters of the $^{2S+1}L_J$ multiplets, and the crystal-field (CF) interaction, which accounts for the breakdown of the degeneracy of the multiplets into the Stark levels and the optical properties of the rare earth ion in the solid.[19]

The CF theory describes the inter-electronic interaction between the electrons of the inner 4f shell of the rare earth ion and the charge of its host ligands, all distributed in a particular local point symmetry. Rare earth ions are properly described in the weak-field limit by using a one-electron CF Hamiltonian, in which a small group of phenomenological parameters allow to reproduce the rare earth energy level diagram. In the framework of the Racah algebra, these phenomenological parameters are numeric coefficients that multiply the tensor operators. This interaction can be described as follows:[20]

$$H_{CF}^{(Even)} = \sum_{k,q} B_q^k (C_q^{(k)}) = \sum_{k=2}^{\leq 6} \sum_{q \geq -k}^{\leq k} B_q^k \left[C_q^{(k)} + (-1)^q C_{-q}^{(k)} \right] + iB'^k_q \left[C_q^{(k)} - (-1)^q C_{-q}^{(k)} \right], \quad (1)$$

where real B_q^k and imaginary B'^k_q CF parameters are radial integrals, while the angular components of the renormalized spherical tensor operators $C_q^{(k)}$ can be precisely calculated with the help of the Racah algebra and the group theory.[20]

When increasing pressure an enhancement of the CF interaction is expected and, in general, increased splitting of the multiplets is observed. In the description of the CF theory, it is useful to define a scalar, rotationally invariant parameter known as the overall CF strength parameter. According to Auzel *et al.*[21,22] and Chang *et al.*,[23] it can be written as

$$S = \left[\frac{1}{3} \sum_k \frac{1}{2k+1} \left\{ |B_0^k|^2 + 2 \sum_{\substack{q \leq k \\ q > 0}} \left(|B_0^k|^2 + |B_0^k|^2 \right) \right\} \right]^{1/2}. \quad (2)$$

Roughly speaking, the maximum splitting of each $^{2S+1}L_J$ multiplet depends linearly on the overall CF strength.

For the D_2 symmetry at the Nd^{3+} sites in garnets, the CF Hamiltonian is

$$H_{CF} = B_0^2 C_0^2 + B_2^2 (C_{-2}^2 + C_2^2) + B_0^4 C_0^4 + B_2^4 (C_{-2}^4 + C_2^4) + B_4^4 (C_{-4}^4 + C_4^4) + B_0^6 C_0^6 + B_2^6 (C_{-2}^6 + C_2^6) + B_4^6 (C_{-4}^6 + C_4^6) + B_6^6 (C_{-6}^6 + C_6^6) \quad (3)$$

with 9 real, non-vanishing CF parameters. However, adequate reproduction of the variation of the energy level positions under pressure is not possible due to the scarcity of available levels in the luminescence spectra measured. Thus, in order to describe the interaction between the rare earth ion and its oxygen ligands in garnets, it is often convenient to assume that the local environment of the rare earth ions is characterized by an orthorhombic distortion of a main cubic symmetry. Thus the complete (free ion + CF) Hamiltonian can be written as

$$H = H_{FREE\text{-}Nd^{3+}} + \{B_0^{4c}[C_0^4 \pm \sqrt{5/14}(C_{-4}^4 + C_4^4)] + B_0^{6c}[C_0^6 \mp \sqrt{7/2}(C_{-4}^6 + C_4^6)]\}_{cubic} + \{B_0^2 C_0^2 + B_2^2 (C_{-2}^2 + C_2^2) + B_0^4 C_0^4 + B_2^4 (C_{-2}^4 + C_2^4) + B_4^4 (C_{-4}^4 + C_4^4) + B_0^6 C_0^6 + B_2^6 (C_{-2}^6 + C_2^6) + B_4^6 (C_{-4}^6 + C_4^6) + B_6^6 (C_{-6}^6 + C_6^6)\}_{non\text{-}cubic}, \quad (4)$$

where two contributions must be taken into account: the cubic symmetry component that can be represented by only the B_0^{4c} and B_0^{6c} CF parameters, since the B_4^{4c} and B_4^{6c} are then obtained by specific ratios,[20] and the non-cubic symmetry component that accounts for the real D_2 symmetry at the

Nd^{3+} sites, and is governed by the appearance of other B_q^k ($k = 2,4,6$; $-k \leq |q| \leq k$; q even) CF parameters and the deviation from the cubic ratios of the resulting fourth and sixth rank CF parameters.

Although 11 real CF parameters appear in this Hamiltonian, seeming to be a more complicated point of view, this description has some evident advantages. As already mentioned, the cubic group splits the $^4I_{9/2}$ ground term into three levels, $\Gamma_6 + 2\Gamma_8$, while keeping the lowest emitting $^4F_{3/2}$ level as a Γ_8 singlet (see Fig. 1). The superimposed non-cubic distortion removes the remaining degeneracy and each Γ_8 cubic-level splits into two Stark doublets to finally give five $^4I_{9/2}$ Stark Z_j levels and two $^4F_{3/2}$ Stark R_j levels (see Fig. 1). The main fact is that, since in a cubic symmetry the $^4F_{3/2}$ emitting multiplet of the Nd^{3+} ion is still a singlet, the non-cubic part of the CF Hamiltonian must be directly responsible for the observed splitting of the $^4F_{3/2}$ state into the R_1 and R_2 Stark emitting levels (ruled by the second rank B_q^2 CF parameters). Thus, this splitting may be used as a rough measurement of the magnitude of the non-cubic distortion from the main cubic crystal-field.

Comparing the R_1-R_2 splitting at ambient conditions ($\sim 100\,cm^{-1}$) to the $^4I_{9/2}$ splitting ($\sim 800\,cm^{-1}$), we can estimate that the contribution to the overall CF strength of the non-cubic distortion is lower than 15% of the overall splitting and, therefore, the main contribution of the overall CF strength ($\sim$85%) comes from the cubic part of the CF Hamiltonian. Moreover, it can be observed that increasing pressure induces different rates of red-shifts of the R_1,$R_2 \rightarrow Z_5$ transitions (see Fig. 3), closing the energy gap between them from around $100\,cm^{-1}$ at ambient pressure to $50\,cm^{-1}$ at 23 GPa. This reduction of the Stark splitting of the $^4F_{3/2}$ multiplet can only be associated with the decrease of the orthorhombic distortion or, in other words, the CF symmetry over the Nd^{3+} site in the garnet lattice becomes more cubic when pressure is increased. Similar results have been found by Hua *et al.* in various garnets.[7] Thus, these facts allow us to make a simplified analysis of the pressure effect on the $^4I_{9/2}$ energy level position using only the cubic part of the CF Hamiltonian and disregarding the effect of the orthorhombic distortion.

In the garnet under study, the $Z_{1\text{-}4}$ Stark levels of the $^4I_{9/2}$ ground state show a very low sensitivity to pressure variations (see Figs. 3 and 4(right)), and their energy separations remain mainly constant, whereas there is a strong variation of the energy position of the Z_5 Stark level that points out larger splittings of the $^4I_{9/2}$ ground multiplet and stronger CF strengths felt by the Nd^{3+} ions as the pressure increases. Although the energy positions of $R_i \rightarrow Z_j$ lines are related to all the CF parameters, due to the Nd^{3+} environment's above-mentioned tendency toward cubic symmetry under pressure, an early analysis might be that the increase in overall CF strength at the Nd^{3+} site must be associated primarily with variations in the cubic part of the CF Hamiltonian. In this framework, a small variation of the cubic B_0^{6c} CF parameter strongly changes the energy position of all Z_j Stark levels, whereas only the energy position of the Z_5 Stark level appears to be particularly dependent on the fourth rank cubic part of the CF Hamiltonian.[9] In fact, increasing the B_0^{4c} by around 50% over its ambient pressure value allows the observed behaviour under pressure of all the $R_j \rightarrow Z_j$ transitions, and hence of all the energy dependence of the Z_j Stark levels, to be reasonably reproduced (see dotted lines in Fig. 4(left)).

In order to delve into this dependency, a brief look must be taken at the theoretical models describing the CF interaction. The simplest, and therefore rather unrealistic, description of the solid and its effect on the RE^{3+} ion is the point charge electrostatic model (PCEM).[24] The fundamental idea is that, associated with each ligand ion, there is a charge concentrated at the atomic position of the ligand, and the electrostatic field acting on every 4f electron of the rare earth ion is generated by this set of point charges. Therefore, the site symmetry of the local environment of the rare earth ion is taken into account through the lattice sum, and the resulting CF parameters are given by[20,25]

$$B_q^k = \sum_{L=1}^{N} (Ze^2)_L \frac{\langle r^k \rangle}{R_L^{k+1}} \sqrt{\frac{4\pi}{2k+1}} Y_{kq}^*(\theta_L, \varphi_L), \tag{5}$$

where $\langle r^k \rangle$ are the radial integrals of the rare earth ion wavefunction; $(Ze)_L$ represents the charge of ligands; R_L their distance from the central rare earth ion; and the spherical harmonics $Y_{kq}^*(\theta_L, \varphi_L)$ describe the angular dependence.

According to Eq. (5), radial dependences in the form $1/R^{k+1}$ are expected for the kth rank CF parameters in the PCEM. Thus an increase of 50% in the cubic fourth rank CF parameter, which means a coupled increase of 76% in the cubic sixth rank CF parameter, translates to a disproportionate decrease of around 22% in the local volume of the RE^{3+}ion, which is absurd for one of the hardest materials, the garnets, in the pressure range under study. This result has to be understood as a failure of the PCEM, which has many approaches, such as neglecting the finite extension of the charge densities of the ligands or the overlap of the wave functions of electrons 4f ions with those of the ligands. That is why the PCEM is taken only as a very rough approximation to the problem, especially for less ionic systems.

Much more realistic results in the simulation of the $^4I_{9/2}$ Stark level fine structure are obtained by using the Superposition Model.[26,27] This model was developed to separate the geometrical and physical information contained in the CF parameters, which are expressed as a sum of individual contributions from the nearest ions in the host crystal lattice, each one being the product of a purely angular part and a radial part that depends on the rare earth-ligand (RE^{3+}-L) distance,

$$B_q^k = \sum_L \overline{B_k}(R_L) g_{k,q}(\theta_L, \varphi_L), \tag{6}$$

where $g_{k,q}$ are normalized spherical harmonic functions, and R_L, θ_L, φ_L locate the position of ligand L in the lattice coordination environment. The so-called intrinsic CF parameter $\overline{B_k}(R_L)$ is characteristic for a specific ligand type, and depends only on the distance between the RE^{3+} ion and the ligand L. A power law dependence is usually assumed in the form,[26,27]

$$\overline{B_k}(R_L) = \overline{B_k}(R_0)(R_0/R_L)^{t_k}, \quad (7)$$

where R_0 is a specific or reference distance, and t_k are power law exponents that reflect the distance dependence of the RE^{3+}-L interaction.

For our simulation, we took a characteristic distance of $R_0 = 2.3$ Å and intrinsic parameters $\overline{B_4}(R_0) = 980\,cm^{-1}$ and $\overline{B_6} = 575\,cm^{-1}$, since these values are quite similar to others reported for the Nd^{3+} ion with oxygen ligands.[28] With these values and a cubic, eight-fold coordinated oxygen structure, it is easy to simulate the effect of pressure forcing a reduction of the RE^{3+}-L distances, while keeping the cubic angular positions fixed. Power law values of $t_4 = 12$ and $t_6 = 6$, previously reported for the Nd^{3+}:YAG system,[27] were used.

At ambient conditions, an Nd^{3+}-O^{2-} distance of 2.363 Å was used and $B_0^{4c} = -2200\,cm^{-1}$ and $B_0^{6c} = 870\,cm^{-1}$ were obtained, giving rise to an overall CF strength $S = 682\,cm^{-1}$. Thus the ambient pressure $^4I_{9/2}$ cubic Stark levels are at 0 (Γ_8), 240 (Γ_8), and 770 (Γ_6) cm^{-1}, respectively (see Fig. 4(left)). On the other hand, the highest pressure conditions at 23 GPa were reached with a Nd^{3+}-O^{2-} distance of 2.278 Å, for which $B_0^{4c} = -3152\,cm^{-1}$ (an increase of ~50%) and $B_0^{6c} = 1041\,cm^{-1}$, resulting in an overall crystal-field strength $S = 994\,cm^{-1}$ and $^4I_{9/2}$ cubic Stark levels at 0 (Γ_8), 281 (Γ_8), and 976 (Γ_6) cm^{-1}. The energy shifts of the $^4I_{9/2}$ cubic Stark levels with pressure can be followed from ambient pressure up to 23 GPa as a function of the overall CF strength in Fig. 4(left, solid lines).

The relevant results of this pressure simulation in the energy range of the $^4I_{9/2}$ splitting in garnet under study can be directly compared with the pressure dependence of the Z_j Stark energy positions obtained from the emission spectra in the Nd^{3+}:CGGG garnet under pressure. Inside the depicted overall CF strength range (700–1000 cm^{-1}), the similar behaviour of the Γ_6 Stark level energy position versus S with those of the pressure dependence of Z_5 energy position becomes evident. Obviously, because the non-cubic distortion has not been taken into account, which contributes with around 100 cm^{-1} (the R lines total splitting), the calculated values of the overall cubic CF strength, and hence the calculated $^4I_{9/2}$ cubic splitting, must be overestimated in some way (~5%–10% appears reasonable value). In fact, assuming a fixed orthorhombic splitting of around 100 cm^{-1} added to both Γ_8 cubic levels in Fig. 4(right), the obtained pressure dependence of $^4I_{9/2}$ level positions is properly reproduced.

With the selected power law values ($t_4 = 12$, $t_6 = 6$), the variation range of the overall CF strength obtained for cubic calculations (700–1000 cm^{-1}) corresponds to a distance reduction of 3% and a relative volume reduction of $\Delta v/v = 8.5\%$. Taking into account the overestimation related to the non-cubic distortion, we can estimate a more reliable and reasonable distance reduction of 2.2%, entailing a relative volume reduction of $\Delta v/v = 6.5\%$.

In summary, under compression, the overall strength of the crystal-field increases, the second-order parameters (and the R-lines splitting) decrease and the ratios of CF parameters become more cubic. Moreover, the cubic B_0^{4c} parameter appears to be mainly responsible for the pressure increase of the energy gap between the Z_5 Stark level and the other $Z_{1\text{-}4}$ levels.

C. Optical pressure calibration

To use the energy positions of the R_1,$R_2 \rightarrow Z_5$ peaks of the Nd^{3+} ion in the CGGG garnet as an indirect measurement of the pressure in the hydrostatic chamber, linear and quadratics fits were carried out in order to obtain a scale in the range of pressures achieved in this work. The results are shown in Table I and, although the quadratic equation provides better fits than linear fits, the latter is used to compare the results of this garnet with the Nd^{3+} ion in YAG and GSGG garnets, and with the Cr^{3+} ion in ruby.[6,9,10] The $R_2 \rightarrow Z_5$ peak in all the garnets is the most sensitive to pressure, with a coefficient of $-10.8\,cm^{-1}$/GPa for the CGGG garnet under study, a slightly smaller value than that found for GSGG, but clearly larger than those of YAG and ruby. The pressure coefficient for the $R_1 \rightarrow Z_5$ peak in CGGG is smaller, similar to other garnets, but larger than ruby. However, due to the broadening of the R_1,$R_2 \rightarrow Z_5$ peaks observed above 15 GPa, more evident in the latter transition, it seems that for the range of pressure analysed the $R_1 \rightarrow Z_5$ line is more suitable for pressure sensor purposes and, due to their low temperature sensitivity,[9] can be used in a wider range of temperatures, if it is wished to introduce this variable into the experiment.

The energies of the R_1,$R_2 \rightarrow Z_5$ peaks of the Nd^{3+} ion in YAG, GSGG, and CGGG garnets are compared in Fig. 5. Analysis of these transitions at different pressures, ranging from ambient pressure up to around 12 GPa, which are the experimental values available in the literature,[9,10] finds different transition energies and R_1-R_2 energy gaps for the three

TABLE I. Linear fit coefficients of the $^4F_{3/2}(R_2) \rightarrow {}^4I_{9/2}(Z_5)$ peak positions as a function of pressure for three different Nd^{3+}-doped garnets and the R-lines of the Cr^{3+}:Al_2O_3 (Ruby). Quadratic coefficient fits are also included for the Nd^{3+}:CGGG garnet.

Transition	Linear fit (cm^{-1}/GPa)	Quadratic fit E_0 (cm^{-1}) + A P(GPa)+B P^2(GPa)^2	Composition
$^4F_{3/2}(R_2) \rightarrow {}^4I_{9/2}(Z_5)$	−11.3		Nd^{3+}:GSGG[9]
$^4F_{3/2}(R_2) \rightarrow {}^4I_{9/2}(Z_5)$	−10.8	$10743.3 - 12.3P - 6.0 \times 10^{-4}P^2$	Nd^{3+}:CGGG (this work)
$^4F_{3/2}(R_2) \rightarrow {}^4I_{9/2}(Z_5)$	−9.9		Nd^{3+}:YAG[10]
$^2E(R_2) \rightarrow {}^4A_2$	−7.56		Cr^{3+}:Al_2O_3 Ruby[6]
$^4F_{3/2}(R_1) \rightarrow {}^4I_{9/2}(Z_5)$	−8.8		Nd^{3+}:GSGG[9]
$^4F_{3/2}(R_1) \rightarrow {}^4I_{9/2}(Z_5)$	−8.8	$10641.0 - 8.4P - 3.7 \times 10^{-4}P^2$	Nd^{3+}:CGGG (this work)
$^4F_{3/2}(R_1) \rightarrow {}^4I_{9/2}(Z_5)$	−7.5		Nd^{3+}:YAG[10]
$^2E(R_1) \rightarrow {}^4A_2$	−7.56		Cr^{3+}:Al_2O_3 Ruby[6]

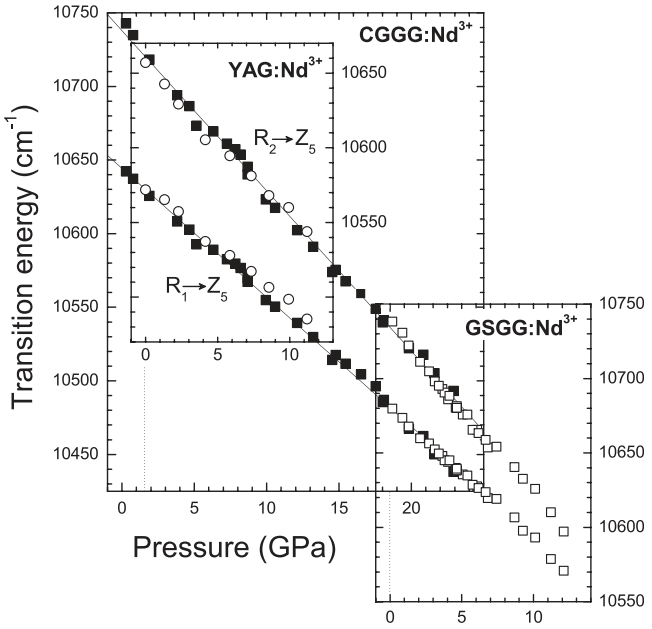

FIG. 5. Pressure evolution of the $R_1,R_2 \rightarrow Z_5$ peaks in Nd^{3+}-doped CGGG (■), GSGG (□),[9] and YAG (○).[10] All graphs use the same scale for the XY axes, but those for YAG and GSGG garnets are shifted in order to fit the same splitting as that of the CGGG garnet under study. Linear fits of the peak transition energies for the CGGG garnet are also included.

garnets. However, a better comparison can be done if the energy gap between the emission peaks is the main variable taken into account. That is why the graphs corresponding to the YAG and GSGG garnets are superimposed and shifted in energy and pressure with respect to that of the CGGG garnets under study, in such a way that the transition energies of the different garnets can be directly compared. Of course, the XY scales are exactly the same for the three graphs.

Two main facts can be inferred from this comparison; first, at ambient conditions, the CGGG garnets has the largest energy gap between the R_1 and R_2 Stark levels, and only at around 1.5 GPa does it have a similar splitting as YAG at ambient pressure. However, the pressure must be increased to around 18.5 GPa to be comparable to the splitting in the GSGG garnet at ambient pressure. Second, the splitting shown in the latter garnet allows us to assume that the energy gap in the CGGG under study is still nonzero up to pressures around 30 GPa, if the hydrostatic conditions are kept using a different pressure transmitting medium. Thus it seems that the CGGG garnet gives the largest dynamic pressure range from ambient pressure up to 30 GPa, if the energies of the $R_1,R_2 \rightarrow Z_5$ emissions peaks of the Nd^{3+} ion are wanted to be used as a pressure measurement inside the DAC.

The key physical factor responsible for this feature has to be found in the local structure of the Nd^{3+} ions in the CGGG garnet at ambient conditions. The initial degree of orthorhombic distortion of the dodecahedral sites is larger when occupied by the Ca^{2+} ions than when occupied by the Gd^{3+} or the Y^{3+} ions, since the ionic radius of the Ca^{2+} ion is larger. In addition, the Nd^{3+} ion could be incorporated as a modifier replacing the Ca^{2+} ion, since both have similar ionic radiuses, obtaining from the crystalline network a stabilized 8-coordinated site with Ge^{4+} ions in the second sphere of coordination to achieve charge neutrality.

IV. CONCLUSIONS

The luminescence spectra as a function of pressure of the $^4F_{3/2} \rightarrow {}^4I_{9/2}$ transition of an Nd^{3+}-doped CGGG garnet, obtained by exciting either by the 488 nm line of an Ar^+ laser or with a 532 nm diode-pumped solid state laser were analysed. At ambient pressure, nine lines were identified according to the conventional notation of the $^4F_{3/2}$ and $^4I_{9/2}$ manifolds. The energy position of these lines is related to a small orthorhombic distortion of a main cubic crystal-field. The behaviour of the energy position of these lines as pressure increases is associated with a reduction in the non-cubic distortion and an increase in the main cubic field, mainly governed by the medium distance B_0^{4c} cubic parameter. This parameter appears to be mainly responsible for the pressure increase of the energy gap between the Z_5 Stark level and the other $Z_{1\text{-}4}$ levels.

Two intense and isolated lines corresponding to $R_1,R_2 \rightarrow Z_5$ transitions centred in the NIR in the interval from 10 600 to 10 800 cm^{-1} are the most sensitive to pressure with linear coefficients of $-10.8\,cm^{-1}$/GPa and $-8.8\,cm^{-1}$/GPa, respectively, both with line shifts higher than that found for the most widely used pressure calibrated standard, the R_1 line of Cr^{3+} in ruby ($-7.56\,cm^{-1}$/GPa). The initial orthorhombic distortions of the Nd^{3+} site seem to be the key factor in having a larger dynamic pressure scale, and the CGGG crystal shows the largest one among garnets studied. These facts, together with the advantages of excitation with a conventional Ar^+ or laser diode and available detectors in this spectral range, make the Nd^{3+}:CGGG garnet a potential candidate to be used as a NIR pressure sensor at room temperature in a diamond anvil cell from ambient to around 30 GPa pressure range.

ACKNOWLEDGMENTS

This work has been partially supported by MICINN (MAT2010-21270-C04-02, The MALTA Consolider CSD2007-0045 and the National Program of Infrastructure), and by EU-FEDER funds. S. F. León-Luis also wishes to thank MICINN for the FPI Grant (BES-2008-003353).

[1]M. I. Eremets, *High Pressure Experimental Methods* (Oxford University Press, 1996).
[2]W. B. Holzapfel and N. S. Isaacs, *High-pressure Techniques in Chemistry and Physics* (Oxford University Press, 1997).
[3]K. Bray, "High pressure probes of electronic structure and luminescence properties of transition metals and lanthanide systems," Top. Curr. Chem. **213**, 1 (2001).
[4]Th. Tröster, "Optical studies of non-metallic compounds under pressure," in *Handbook on the Physics and Chemistry of Rare-earths*, edited by K. A. Gschneidner, Jr., J.-C. G. Bünzli, and V. K. Pecharsky (Elsevier Science B.V., 2003), Vol. 33, p. 515.
[5]J. D. Barnett, S. Block, and G. J. Piermarini, Rev. Sci. Instrum. **44**, 1 (1973).
[6]K. Syassen, High Press. Res. **28**, 75 (2008).
[7]H. Hua, S. Mirov, and Y. Vohra, Phys. Rev. B **54**, 6200 (1996).
[8]A. Kaminska, P. Kaczor, A. Durygin, A. Suchocki, and M. Grinberg, Phys. Rev. B **65**, 104106 (2002).
[9]S. F. León-Luis, J. E. Muñoz-Santiuste, V. Lavín, and U. R. Rodríguez-Mendoza, Opt. Express **20**, 10393 (2012).
[10]S. Kobyakov, A. Kaminska, A. Suchocki, D. Galanciak, and M. Malinowski, Appl. Phys. Lett. **88**, 234102 (2006).

[11]A. Kaminska, R. Buczko, W. Paszkowicz, H. Przybylinska, E. Werner-Malento, A. Suchocki, M. Brik, A. Durygin, V. Drozd, and S. Saxena, Phys. Rev. B **84**, 075483 (2011).
[12]F. Ramos, H. Loro, E. Camarillo, J. García-Solé, A. A. Kaminskii, and U. Caldiño, Opt. Mater. **12**, 93 (1999).
[13]J. B. Gruber, M. E. Hills, C. A. Morrison, G. A. Turner, and M. R. Kotka, Phys. Rev. B **37**, 8564 (1988).
[14]U. Hömmerich and K. L. Bray, Phys. Rev. B **51**, 12133 (1995).
[15]N. A. Eskov, V. V. Osiko, A. A. Sobol, M. I. Timoshechkin, T. I. Butaeva, C. Ngok, and A. A. Kaminskii, Izv. Akad. Nauk. SSR Ser. Neorg. Mater. **14**, 2254 (1978).
[16]U. G. Caldiño, M. Voda, F. Jaque, J. García-Solé, and A. A. Kaminskii, Chem. Phys. Lett. **213**, 84 (1993).
[17]U. G. Caldiño, L. E. Bausa, J. García-Solé, F. Jaque, A. A. Kaminskii, A. V. Butashin, and B. V. Mill, J. Phys. IV France **4**, C4–389 (1994).
[18]A. Abragam and B. Bleaney, *Electron Paramagnetic Resonance of Transition Ions* (Dover Publications, Inc., New York, 1970).
[19]G. Huber, K. Syassen, and W. B. Holzapfel, Phys. Rev. B **15**, 5123 (1977).
[20]C. Görller-Walrand and K. Binnemans, "Rationalization of crystal-field parametrization," in *Handbook on the Physics and Chemistry of Rare-earths*, edited by K. A. Gschneidner, Jr. and L Eyring (Elsevier Science B.V., 1996), Vol. 23, p. 121).
[21]F. Auzel, Mater. Res. Bull. **14**, 223 (1979).
[22]F. Auzel and O. L. Malta, J. Phys. (Paris) **44**, 201 (1983).
[23]N. C. Chang, J. B. Gruber, R. E. Leavitt, and C. A. Morrison, J. Chem. Phys. **76**, 3877 (1982).
[24]H. Bethe, Annalen der Physik. **395**, 133 (1929).
[25]B. G. Wybourne, *Spectroscopic Properties of Rare Earths* (Wiley-Interscience, New York, 1965).
[26]D. J. Newman and B. Ng, Rep. Prog. Phys. **52**, 699 (1989).
[27]D. J. Newman and B. Ng, *Crystal-Field Handbook* (Cambridge University Press, 2000).
[28]D. Garcia and M. Faucher, "Crystal field in non-metallic (rare earth) compounds," in *Handbook on the Physics and Chemistry of Rare Earths*, edited by K. A. Gschneidner, Jr. and L. Eyring (Elsevier Science B. V., 1995), Vol. 21, p. 263.